Supplementary Material to "Optical characterization of a single molecule complete spatial orientation using intra-molecular triplet-triplet absorption"

Remigiusz Trojanowicz,[†] Ludovic Douillard,[†] Lydia Sosa Vargas,[‡] Fabrice Charra,[†] and Simon Vassant[*,†]

†*Université Paris-Saclay, CEA, CNRS, SPEC, F-91191, Gif-sur-Yvette, France*

‡*Sorbonne Université, CNRS, Institut Parisien de Chimie Moléculaire (IPCM), F-75005,*
Paris, France

E-mail: simon.vassant@cea.fr

1. Autocorrelation function for a 3-level system with reverse intersystem crossing

The functional form of the correlation function $g^{(2)}(\tau)$ can be determined fully by the rates involved in the level scheme of the emitter. We use the level scheme described in Figure 1c of the main article.

The correlation function is given by[1] :

$$g^{(2)}(\tau) = \frac{S_1(\tau)}{S_1^{ss}} \tag{1}$$

where $S_1(\tau)$ is the population evolution of the excited singlet level, and S_1^{ss} is the steady-state occupation of the excited level. We thus need to derive the master equation for $S_1(t)$ from the rate equations.

The population of the three states (ground singlet S_0, excited single S_1 and triplet state T_1) are given by a first order differential equation system :

$$
\begin{pmatrix} n_{\dot{S_0}} \\ n_{\dot{S_1}} \\ n_{\dot{T_1}} \end{pmatrix} = \begin{bmatrix} -k_{12} & k_{21} & k_{31} \\ k_{12} & -(k_{23}+k_{21}) & k_{32} \\ 0 & k_{23} & -(k_{31}+k_{32}) \end{bmatrix} \cdot \begin{pmatrix} n_{S_0} \\ n_{S_1} \\ n_{T_1} \end{pmatrix}, \tag{2}
$$

The solutions of such systems are of the form $\sum_i \nu_i \exp(\gamma_i t)$, where ν_i are the eigenvectors, γ_i the eigenvalues of the matrix. The index i runs over the number of eigenvalues of the system. The eigenvalues γ_i are the solution of:

$$
det(M - \gamma I) = 0, \tag{3}
$$

where M is the central matrix of Eq. 2, and I is the identity matrix. After some algebra we end up with the following third degree equation :

$$
\gamma^3 + \gamma^2(k_{12}+k_{21}+k_{23}+k_{32}+k_{31}) + \gamma[k_{12}(k_{31}+k_{32}+k_{23})+k_{21}(k_{31}+k_{32})+k_{31}k_{23}] = 0 \tag{4}
$$

This yields 3 eigenvalues :

$$
\gamma_1 = 0, \tag{5}
$$
$$
\gamma_2 = \frac{-P - \sqrt{P^2 - 4Q}}{2}, \tag{6}
$$
$$
\gamma_3 = \frac{-P + \sqrt{P^2 - 4Q}}{2}, \tag{7}
$$

with :

$$P = k_{12} + k_{21} + k_{23} + k_{32} + k_{31}, \tag{8}$$

$$Q = k_{12}(k_{31} + k_{32} + k_{23}) + k_{21}(k_{31} + k_{32}) + k_{31}k_{23}. \tag{9}$$

Note that the eigenvalues γ_2 and γ_3 are negative. The next step is to get the eigenvector ν_i, which are found by writing:

$$(M - \gamma_i I)\nu_i = 0 \tag{10}$$

The first eigenvector is found by looking at the population at infinite time, and considering that the sum of the populations has to be unity:

$$n_{S_0} + n_{S_1} + n_{T_1} = 1 \tag{11}$$

The second and third eigenvector are found by considering that at time t=0, the system is in the ground state ($n_{S_0}=1$, $n_{S_1}=0$, $n_{T_1}=0$).

We can then write the full time dependence of excited state :

$$n_{S_1} = \frac{k_{12}(k_{31} + k_{32})}{\gamma_2\gamma_3} + \frac{k_{12}(\gamma_2 + k_{31} + k_{32})}{\gamma_2(\gamma_2 - \gamma_3)}\exp(\gamma_2 t) + \frac{k_{12}(\gamma_3 + k_{31} + k_{32})}{\gamma_3(\gamma_3 - \gamma_2)}\exp(\gamma_3 t) \tag{12}$$

The expression of $g^{(2)}(\tau)$ is given by :

$$g^{(2)}(\tau) = \frac{S_1(\tau)}{S_1^{ss}} = 1 + \frac{\gamma_3(\gamma_2 + k_{31} + k_{32})}{(k_{31} + k_{32})(\gamma_2 - \gamma_3)}\exp(\gamma_2\tau) + \frac{\gamma_2(\gamma_3 + k_{31} + k_{32})}{(k_{31} + k_{32})(\gamma_3 - \gamma_2)}\exp(\gamma_3\tau) \tag{13}$$

We define the contrast A as :

$$A = \frac{\gamma_2(\gamma_3 + k_{31} + k_{32})}{(k_{32} + k_{31})(\gamma_3 - \gamma_2)}. \tag{14}$$

For notation commodity, we define $\lambda_i = -\gamma_i$ and arrive to Equation (2) of the article :

$$g^{(2)}(\tau) = 1 - (1 + A)\exp(-\lambda_2\tau) + A\exp(-\lambda_3\tau) \qquad (15)$$

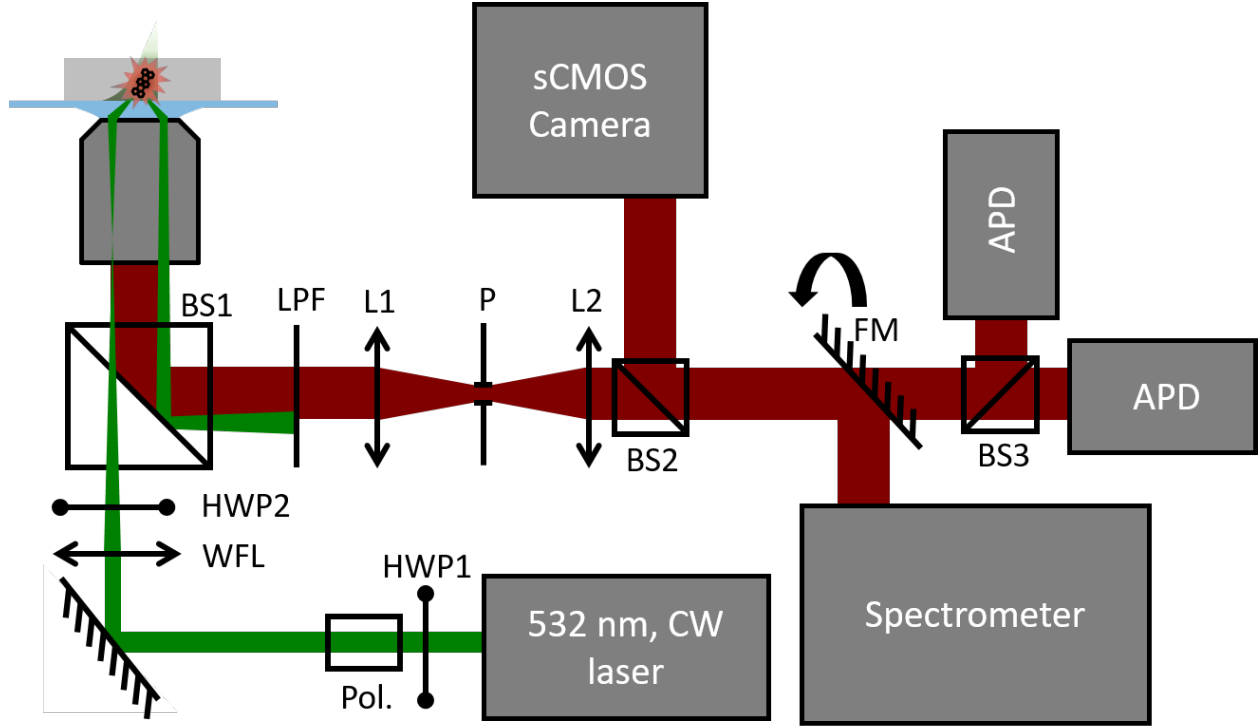## 2. Simplified experimental setup scheme

Figure S1: Simplified schematics of the experimental setup. See text for details.

A simplified scheme of the setup is presented in Fig. S1. The output of a continuous wave, 532nm laser passes through a motorized half-wave plate (HWP1) and a polarizer (Pol.) for power control. The laser mode is cleaned using a polarization maintaining single mode fiber to get a gaussian beam profile (not represented in Fig. S1). We use a 532nm line-filter (Semrock LL01-532-12.5) to remove any unwanted parasitic light and further clean the polarization with a Glan-Thompson polarizer (not represented in Fig. S1). We can then adjust the linear polarization using another motorized half-wave plate (HWP2) before entering the microscope objective. We weakly focus the beam with a 50 cm wide-field

4

lens (WFL) on the side of the back-focal plane of an oil-immersion microscope objective (Olympus, 100X, NA 1.3) to achieve total-internal reflection at the sample with a point-spread function of around 1.5μm diameter, ensuring a constant excitation power in regards to small mechanical drifts. Light coming back from the sample is collected by the same objective, and is reflected by a broadband T:30/R:70 beamsplitter (Thorlabs BS022, BS1 in Fig. S1). The excitation light is suppressed using two long pass filter (Semrock LP03-532RE-25, LPF in Fig. S1). We use a 1:1 telescope (L1-L2) to place a 50 μm pinhole (P) in a conjugated plane of the sample image plane for confocal detection. Afterwards, we send 10% of the light to a sCMOS camera (Hamamatsu Orca Flash 4.0) with a T:90/R:10 Thorlabs beamsplitter BS025, BS2 in Fig. S1). The remaining 90% are sent to either a spectrometer (Andor Shamrock 193i) equipped with a CCD camera (Andor iDus DU401A-BVF) or to a Hanbury Brown Twiss (HBT) detection. The HBT setup is made of a 20cm lens to focus on the detectors (not represented in Fig. S1), a T:50/R:50 non polarizing beamsplitter (Thorlabs BS013, labeled BS3 in Fig. S1), two band-pass filters (Semrock 632/148 BrightLine HC) and two avalanche photodiodes (Excelitas SPCM-AQRH-16). Counts from the detectors are registered using a PicoHarp 300 time-tagged-time-resolved electronics. Finally, the sample is mounted on a three dimensional piezo-stage (MadCityLabs) for precise focus and alignment.

Measurement Procedure. We start by finding a smooth area on the sample using a bottom white light illumination (not shown in Fig. S1). The thickness of the pT film is then checked by Atomic-Force Microscopy (not shown in Fig. S1), and we select only areas with a thickness in the 20-30nm range.

We then record a hyperspectral fluorescence map of that area and check the spectrum of the different fluorescent molecules. A majority of them show a typical emission peak around 578nm, with a vibrational replica centered around 630nm, in agreement with Ref.[2] Some other molecules showing red-shifted spectrum (by 16 to 20nm) are discarded from the analysis.

As reported in Ref.[3], we observe doughnut-shaped spots on the camera suggesting a

vertical orientation of the molecule above the substrate plane. To confirm this we perform a quick input polarization scan at constant excitation power. Molecules behaving strangely at that stage are discarded.

Afterwards, we align the input polarization to the optimal excitation of the molecule, and perform a measurement where we subject the molecule to a ramp in excitation power, starting from low power, to a maximum of around 370kW/cm^2, and then decreasing again to the minimum input power. A majority of molecules show a clear saturation behavior with no hysteresis. Molecules showing instability or hysteresis are discarded.

Finally, we adjust the count rate at optimal excitation to be close to 1MHz, and perform an excitation polarization scan.

All the previously described experiments where we vary excitation polarization or power were recorded in a time-tagged-time-resolved mode using the HBT detection, while continuously varying either excitation power or polarization.

On a count of 50 molecules, only 16 passed all the criteria and survived the whole experimental procedure. We then bin the photons by 200ms intervals and construct the $g^{(2)}(\tau)$ function for each, corresponding to an average power or an average incident angle depending on the type of scan (power scan or polarization scan). For each 200ms time segment, we perform a fit using equation 15 allowing us to extract λ_2, λ_3 and A. The measured count rate R is given by the number of detected photons divided by the time segment duration. For all measurements, $g^{(2)}(\tau = 0)$ is well below 0.5 (typically 0.1 to 0.2), ensuring that we observe a single molecule.

3. Para-Terphenyl Preparation and Topography

Sample preparation. To prepare our samples, we use pT from commercial source (Sigma-Aldrich, $\geq$99.5% (HPLC)), while Tr molecule are synthesized following the procedure described in Ref.[4] The samples are prepared on clean glass coverslips (175 μm thickness) following the procedure of Ref.[3] We can find large pT domains with thicknesses below 30nm (in-situ control by atomic force microscopy measurements) containing a low density of Tr molecules: typically one Tr molecule per 5x5μm^2.

Typical shear-force Atomic-Force Microscopy (AFM) image of the thin para-terphenyl on glass is illustrated in Figure S2. The images were acquired using a home-made AFM head. The tip is a pulled glass fiber glued on a tuning fork. The oscillation frequency of the fork is used to keep the tip at constant height above the surface using a setpoint of -1Hz. The sample is then scanned and the height recorded using a Nanonis electronic controller.

The image in Figure S2 was corrected using Gwyddion, by applying line by line correction using a linear fit. Then a mask was applied to ignore the lowest height levels, and another line by line correction was applied. Similar to what is observed in the work of Pfab et al.,[3] the para-terphenyl film has defects showing preferential directions that allows for height measurements. The absence of para-terphenyl is confirmed by looking at Raman scattering of para-terphenyl that is absent in such low height areas. A cross-section on the AFM image shows the height of the film that is around 20nm for this particular area. For all molecules, the film thickness was checked this way to be below 30nm.
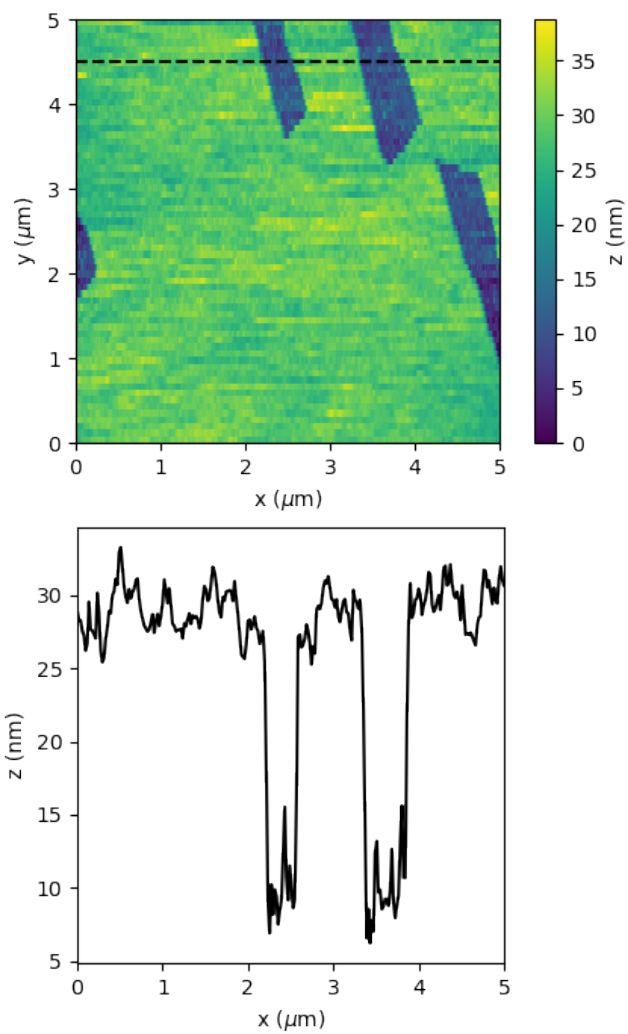
Figure S2: Atomic Force Microscopy scan of Molecule 3 area (top), with a cross-section (bottom) corresponding to the horizontal dashed line in the top image.

4. Terrylene Fluorescence Spectrum

A typical uncorrected fluorescence spectrum is shown in Figure S3, which is similar to previous reports in the literature.[2] The spectra of all the other molecules have the same shape and maximum wavelength. Molecules showing differences with this typical spectra are discarded from the study.
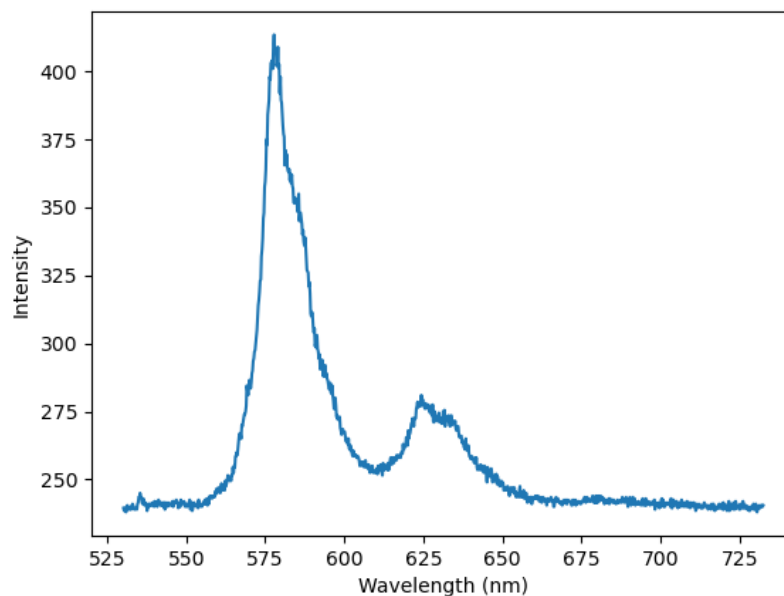

Figure S3: Typical uncorrected fluorescence signal from a single Terrylene molecule.

5. Experimental determination of the intensity auto-correlation function $g^{(2)}(\tau)$

We present in Figure S4 the $g^{(2)}(\tau)$ function obtained from 0.2s time segment of a power scan. Panels a) to c) correspond to increasing excitation power. As illustrated in Ref.[5] and discussed in details in Ref.,[6] start-stop measurement provide a good approximation of the $g^{(2)}(\tau)$ function for time delays shorter than a few lifetime of the emitter. For longer time delays however, the start-stop measurements do not correctly describe the $g^{(2)}(\tau)$ function. In practice, we use the start-stop measurements to build the $g^{(2)}(\tau)$ function for short times delays (≤ 100 ns). For longer time delays (≥ 500 ns), we build time traces from the two APD signals and use a cross-correlation algorithm (multipletau[7]). We are thus able to reconstruct the $g^{(2)}(\tau)$ from picosecond to seconds time delays. The experimental data is fitted with equation 15 and 50, resulting in the determination of λ_2, λ_3 and A. The dashed curves in Figure S4 are the results of such fits. At the same time, we control that $g^{(2)}(\tau = 0)$ is well below 0.5, indicating that we observe a single emitter. The residual value of $g^{(2)}(\tau = 0)$ (between 0.1 and 0.2 depending on the excitation power) is in good agreement with the signal to noise ratio of our measurements.
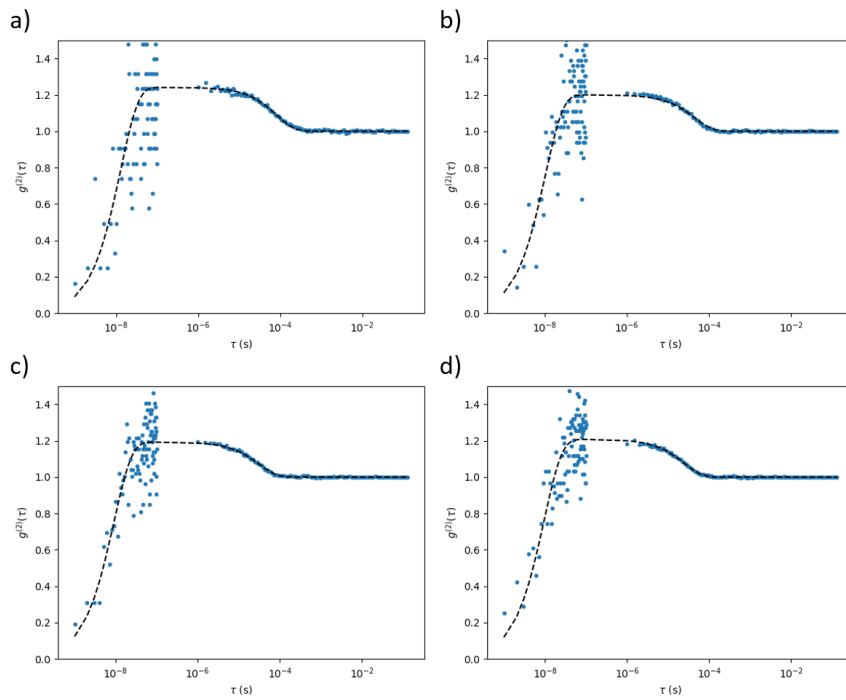
Figure S4: Antibunching curves at different excitation powers : a)2 mW, b) 3 mW, c)4 mW d) 6 mW. Dots represent experimental data while dashed lines are the result of a fit.

6. Global Fit Function

6.1 Determination of the excitation angle of incidence

We determine the angle of incidence experimentally from an image of the back-focal plane. The laser is first expanded (to fill the back-aperture of the objective) and sent at normal incidence into the microscope objective with the sample mounted. This way we obtain a circular image of the back-focal plane (BFP) of the microscope objective with a good contrast, showing an annulus of higher intensity, typical of total internal reflection above the critical angle θ_c. The outer limit of the BFP corresponds to the maximum collection angle given by the numerical aperture of the objective. We use image processing routine from the skimage Python toolkit to adjust circles to these camera images, and extract the central point of the BFP, as well as the circles corresponding to θ_c and θ_{max}. We use an index of 1.5157 for glass and 1 for air, giving $\theta_c = 41.28°$ and $\theta_{max} = 59°$ We use the BFP center and these two angles to convert the camera pixels into angles.

Then we image the laser focused in the BFP by a 50cm wide field lens as used in the experiment. We obtain a gaussian focused beam in the BFP. We calculate from the maximum location of the gaussian the angle of incidence of our beam, giving a result of $\theta_i = 51.4°$
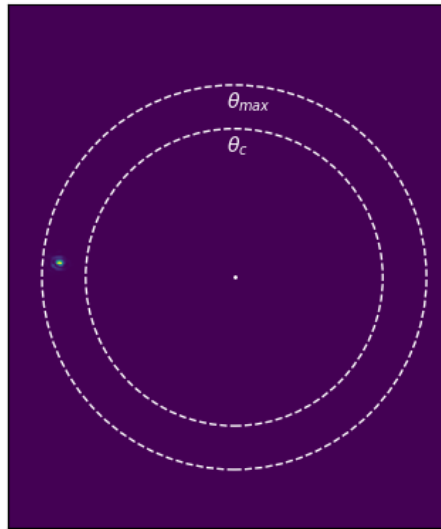
Figure S5: Back-focal plane image of the incident beam during the single molecule experiments. The dashed circle indicates the maximum collection angle $\theta_{max} = 59°$ and the critical angle $\theta_c = 41.28°$. The centre of the BFP $\theta = 0°$ is indicated by a dot.

6.2 Excitation Electromagnetic Field Distribution

We give details on the calculations of the incident electric field distribution in the 3 layer system consisting of a glass substrate, a thin para-Terphenyl film of thickness h, and an air superstrate. Calculation are based on D. Axelrod article.[8] The refractive indexes are 1.8 for pT, 1.5157 for glass (BK7) and 1 for air. The substrate plane is considered in the x-y plane, and z is the propagation direction. Light is incident from the glass side.

We define :

$$k_0 = 2\pi/\lambda, \tag{16}$$

the vacuum wave-vector, with $\lambda = 532$nm the incident wavelength. The plane wave is incident at an angle θ_1 from the normal, so that :

$$k_x = n_1 k_0 \sin \theta_1, \tag{17}$$

with n_1 the substrate index (glass, 1.5157). k_x is constant through the propagation. We can now calculate the k_z component in all the layers :

$$k_{zi} = \sqrt{\epsilon_i k_0^2 - k_x^2} \tag{18}$$

with i ranging from 1 to 3, and $\epsilon_i = n_i^2$

The angle of refraction in layer 2 and 3, are given by :

$$\theta_i = \arctan(k_x/k_{zi}) \tag{19}$$

Now we need to define the Fresnel coefficients at the different interfaces, and be careful

that we'll consider Electric field, so that we get:[9]

$$r_{ij}^{TM} = \frac{\epsilon_j k_{zi} - \epsilon_i k_{zj}}{\epsilon_j k_{zi} + \epsilon_i k_{zj}} \tag{20}$$

$$t_{ij}^{TM} = \frac{2\epsilon_j k_{zi}}{\epsilon_j k_{zi} + \epsilon_i k_{zj}} \sqrt{\frac{\epsilon_i}{\epsilon_j}} \tag{21}$$

$$r_{ij}^{TE} = \frac{k_{zi} - k_{zj}}{k_{zi} + k_{zj}} \tag{22}$$

$$t_{ij}^{TE} = \frac{2k_{zi}}{k_{zi} + k_{zj}} \tag{23}$$

The overall reflection coefficients are then given by:[10]

$$r_{13}^{TM} = \frac{r_{12}^{TM} + r_{23}^{TM} e^{2ik_{z2}h}}{1 + r_{12}^{TM} r_{23}^{TM} e^{2ik_{z2}h}} \tag{24}$$

$$r_{13}^{TE} = \frac{r_{12}^{TE} + r_{23}^{TE} e^{2ik_{z2}h}}{1 + r_{12}^{TE} r_{23}^{TE} e^{2ik_{z2}h}} \tag{25}$$

Now we define interface 1 at -h, and interface 2 at 0. The expression for the electric fields in medium 1 (incident, glass) are given by :

$$E_{1x} = \cos\theta_1 \left[e^{ik_{z1}(z+h)} - r_{13}^{TM} e^{-ik_{z1}(z+h)} \right] \tag{26}$$

$$E_{1y} = e^{ik_{z1}(z+h)} + r_{13}^{TE} e^{-ik_{z1}(z+h)} \tag{27}$$

$$E_{1z} = \sin\theta_1 \left[e^{ik_{z1}(z+h)} + r_{13}^{TM} e^{-ik_{z1}(z+h)} \right] \tag{28}$$

The expression for the electric fields in medium 2 (film, pT) are given by:

$$E_{2x} = \frac{\cos\theta_2 \left[t_{12}^{TM} e^{ik_{z2}h} e^{ik_{z2}z} - r_{23}^{TM} e^{-ik_{z2}z} \right]}{1 - r_{23}^{TM} r_{21}^{TM} e^{2ik_{z2}h}} \tag{29}$$

$$E_{2y} = \frac{t_{12}^{TE} e^{ik_{z2}h} e^{ik_{z2}z} + r_{23}^{TE} e^{-ik_{z2}z}}{1 - r_{23}^{TE} r_{21}^{TE} e^{2ik_{z2}h}} \tag{30}$$

$$E_{2z} = \frac{\sin\theta_2 \left[t_{12}^{TM} e^{ik_{z2}h} e^{ik_{z2}z} + r_{23}^{TM} e^{-ik_{z2}z} \right]}{1 - r_{23}^{TM} r_{21}^{TM} e^{2ik_{z2}h}} \tag{31}$$

15

Finally the fields in medium 3 are given by:

$$E_{3x} = \frac{\cos\theta_3 \left[t_{12}^{TM} t_{23}^{TM} e^{ik_{z2}h} e^{ik_{z3}z} \right]}{1 - r_{23}^{TM} r_{21}^{TM} e^{2ik_{z2}h}} \tag{32}$$

$$E_{3y} = \frac{t_{12}^{TE} t_{23}^{TE} e^{ik_{z2}h} e^{ik_{z3}z}}{1 - r_{23}^{TE} r_{21}^{TE} e^{2ik_{z2}h}} \tag{33}$$

$$E_{3z} = \frac{\sin\theta_3 \left[t_{12}^{TM} t_{23}^{TM} e^{ik_{z2}h} e^{ik_{z3}z} \right]}{1 - r_{23}^{TM} r_{21}^{TM} e^{2ik_{z2}h}} \tag{34}$$

Plotting this equations and comparing them with BEM calculations[11] yields a very good agreement.
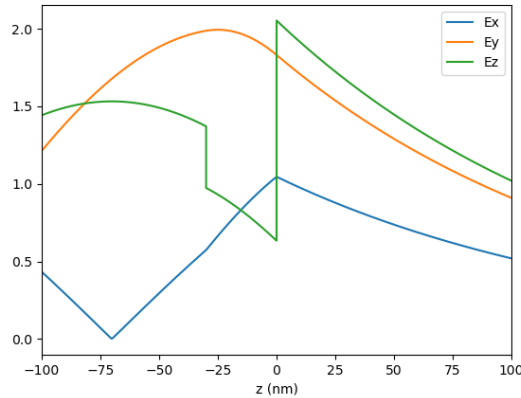

Figure S6: Electric field profiles for the excitation beam at 532nm. The pT film is located bewteen -30nm and 0nm, with glass on the left and air on the right.We consider pT as an isotropic medium of index 1.8.

6.3 Dipoles orientations

We give here the formulas used for the dependence of the power absorbed by the dipole as a function of the incident polarization, using the angles defined in Figure 1 of the main article.

The interaction of the excitation field with the absorption dipole moment of the molecule is given by $|\boldsymbol{\mu} \cdot \mathbf{E}|^2$, where $\boldsymbol{\mu}$ is the dipole moment associated with the transition.

The electric field components are given in the previous section of the Supplementary

16

Material and they vary with the input polarization angle ψ as :

$$E_x = E_{2x}(h) \cos \psi \tag{35}$$

$$E_y = E_{2y}(h) \sin \psi \tag{36}$$

$$E_z = E_{2z}(h) \cos \psi \tag{37}$$

We call $\mathbf{D}$ the singlet-singlet absorption dipole with components D_x, D_y, D_z:

$$D_x = \sin \theta \cos \phi \tag{38}$$

$$D_y = \sin \theta \sin \phi \tag{39}$$

$$D_z = \cos \theta \tag{40}$$

We now want to calculate the cartesian coordinates of the triplet-triplet absorption dipole moment that is orthogonal to the single-singlet absorption dipole moment. Physically, the molecule has its long axis aligned with the singlet-singlet absorption dipole, and is free to rotate around that axis, and so is that orthogonal triplet-triplet absorption dipole moment. To implement this in our coordinate system, we need to use a rotation matrix around the singlet-singlet absorption dipole.

We start by defining an orthogonal absorption dipole components by :

$$T_{x0} = \sin(\theta + \pi/2) \cos \phi \tag{41}$$

$$T_{y0} = \sin(\theta + \pi/2) \sin \phi \tag{42}$$

$$T_{z0} = \cos(\theta + \pi/2) \tag{43}$$

This vector is orthogonal to the singlet-singlet dipole and in the plane defined by ϕ. It is then free to rotate by an angle α around $\mathbf{D}$. Its components can be calculated using a rotation

matrix. This gives:

$$
\begin{bmatrix} T_{x\alpha} \\ T_{y\alpha} \\ T_{z\alpha} \end{bmatrix} = \begin{bmatrix} D_x^2(1-c)+c & D_xD_y(1-c)-D_zs & D_xD_z(1-c)+D_ys \\ D_xD_y(1-c)+D_zs & D_y^2(1-c)+c & D_yD_z(1-c)-D_xs \\ D_xD_z(1-c)-D_ys & D_yD_z(1-c)+D_xs & D_z^2(1-c)+c \end{bmatrix} \begin{bmatrix} T_{x0} \\ T_{y0} \\ T_{z0} \end{bmatrix}, \quad (44)
$$

where we define c and s as :

$$
\begin{aligned}
c &= \cos\alpha & (45) \\
s &= \sin\alpha & (46)
\end{aligned}
$$

6.4 Dead time correction

The non linearity of the Excelitas SPCM-AQRH-16 is very close to 1 for the considered count rates (maximum of $\approx$ 1MHz for each detector). We only consider dead time correction by applying the following formula for the corrected count rate R_{corr} :

$$
R_{corr} = \frac{R}{1 - R\tau_D}, \quad (47)
$$

where R is the measured count rate of one detector, and τ_D is the deadtime of the detector (80 ns).

6.5 Background correction

The count rate is corrected by experimental measurement on para-terphenyl thin film close to the molecule, and subjected to the same power scan and polarization scan.

The intensity auto-correlation function $(g^{(2)}(\tau))$ is corrected using the procedure described in Ref.[12]

Let us call the measured intensity $\tilde{I}(t)$ and define it as :

$$\tilde{I}(t) = I(t) + B, \tag{48}$$

where I(t) is the pure single emitter emitted intensity and B the background.

Now if one assumes that B is a fraction of the intensity :

$$B = b\langle I(t)\rangle, \tag{49}$$

then (1/b) can be seen as the signal to noise ratio, that we can get from the experimental data. We end up with :

$$\tilde{g}^{(2)}(\tau) = \frac{g^{(2)}(\tau) + 2b + b^2}{1 + 2b + b^2} \tag{50}$$

6.6 Starting values for ϕ

The fit automatically finds solutions when using starting values taken from the literature. The angles θ and α do not need particular precautions for the starting value. However, the starting value of ϕ is not trivial. For this parameter, we had to make fits for different starting values, ranging from 0 to 360 degrees, and check the residuals. There are clearly two plateaus of low residuals. Both are around 100 degrees wide. Depending on the fitted molecule, one or the other has a lower residual value, and was chosen as a starting point for that molecule.
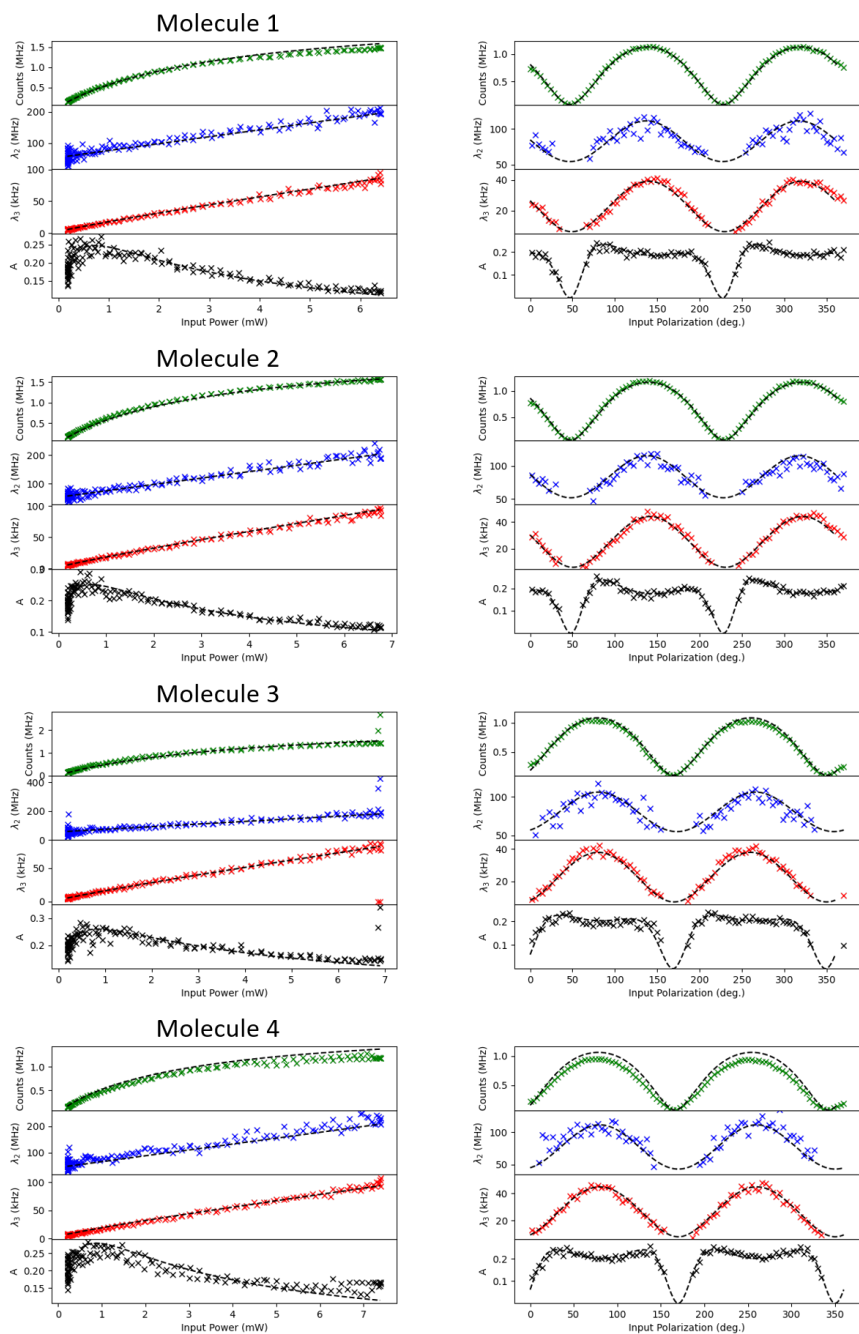
6.7 Global fit results for the 16 molecules

Figure S7: Global fit results for molecule 1 to 4. Left: power scans. Right: Polarization scans.
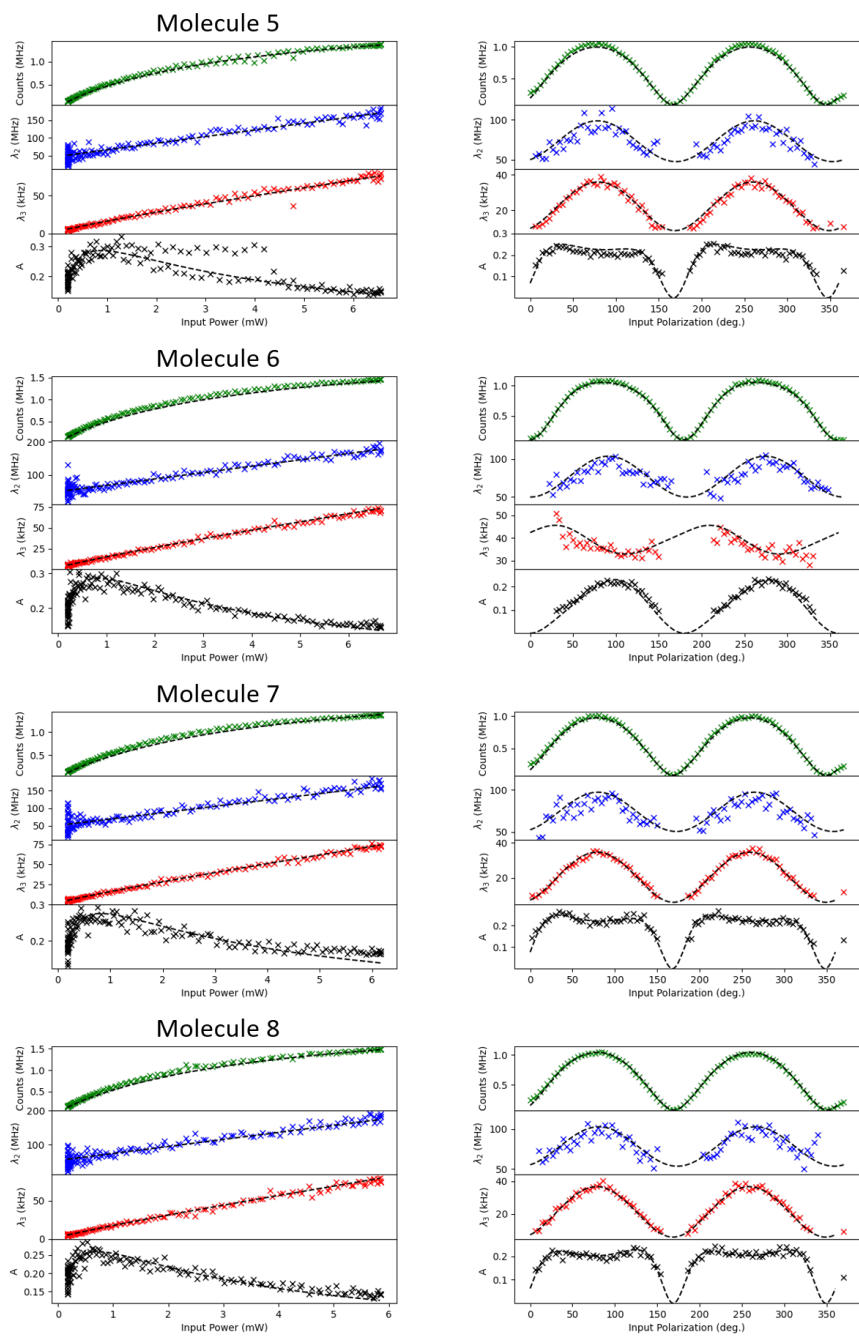
Figure S8: Global fit results for molecule 5 to 8. Left: power scans. Right: Polarization scans.
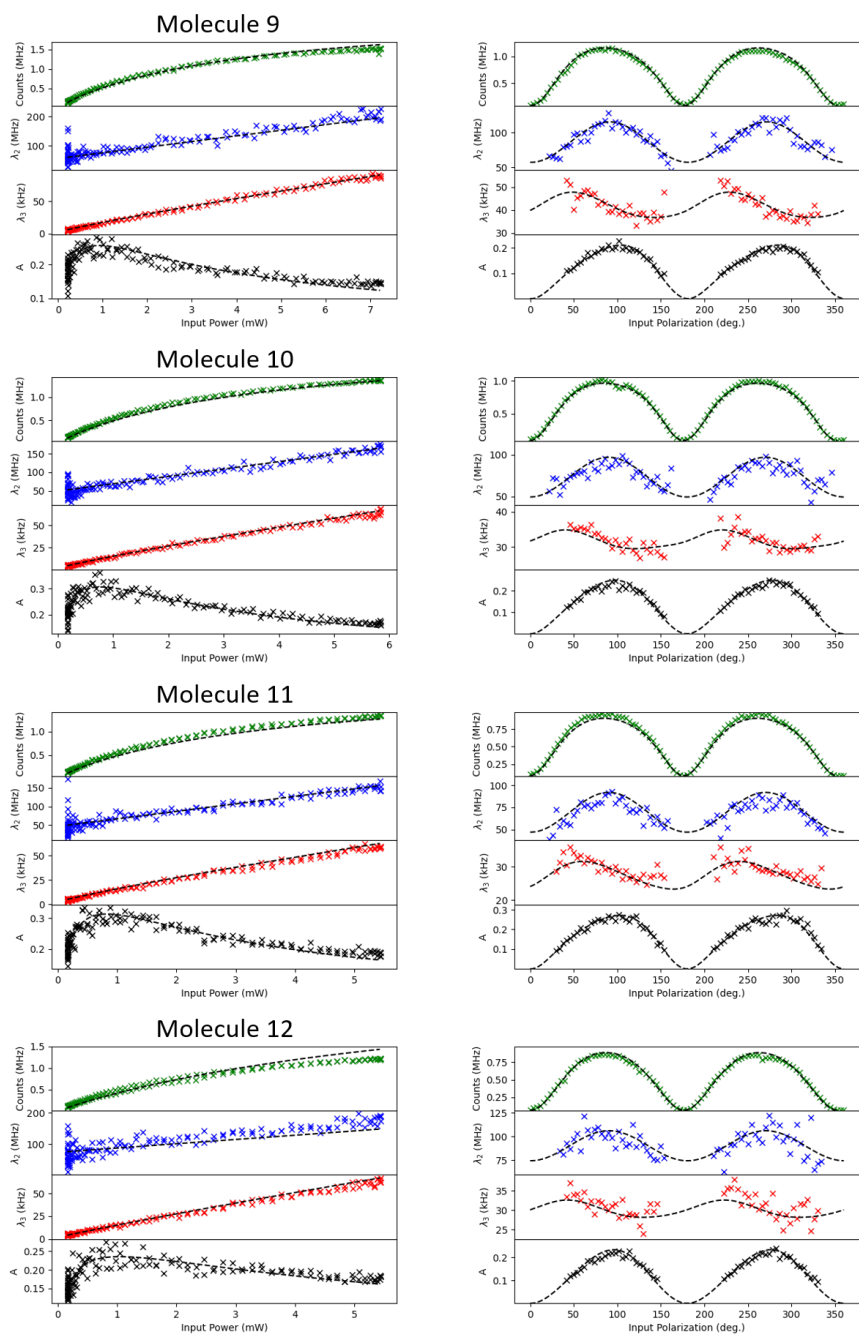
Figure S9: Global fit results for molecule 9 to 12. Left: power scans. Right: Polarization scans.
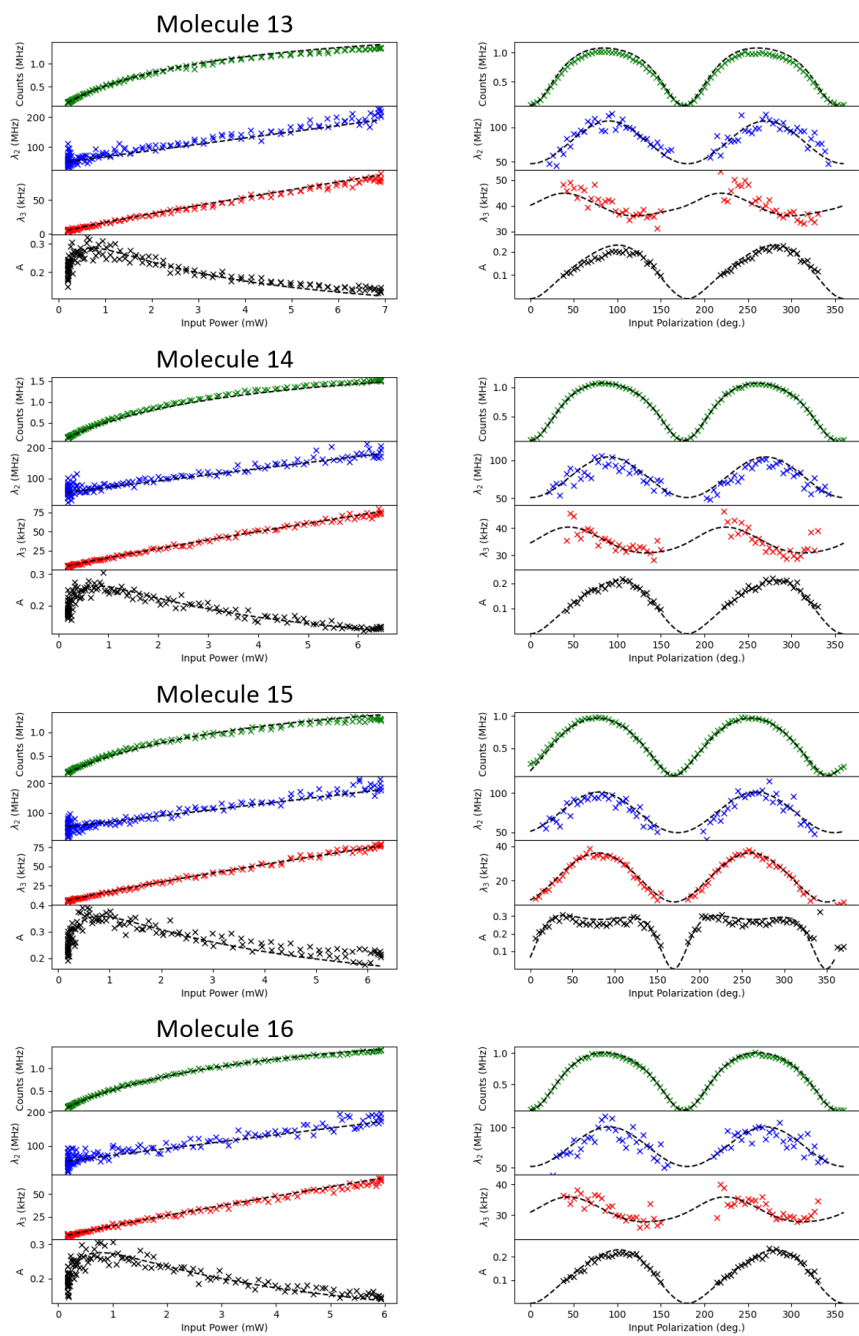
Figure S10: Global fit results for molecule 13 to 16. Left: power scans. Right: Polarization scans.

6.8 Orientation of the molecules

The angles found for the 16 molecules are presented in Figure S11. As expected from the doughnut shape in the image plane, terrylene molecules are standing almost vertical on the substrate, inside the pT film, with values of θ (angle between the singlet transition dipole moment and the normal of the surface) ranging from 6 to 30°. As mentioned in the article, it is difficult to give a physical meaning in the values of the other angles, as the pT crystal domain orientations are unknown, and not directly accessible. Nevertheless, all angles are obtained with rather small confidence intervals, and gives the full orientation of the molecule. The angles θ and ϕ give the orientation of the singlet dipole transition moment, while α gives the rotation angle of the molecule plane around the singlet dipole transition moment.
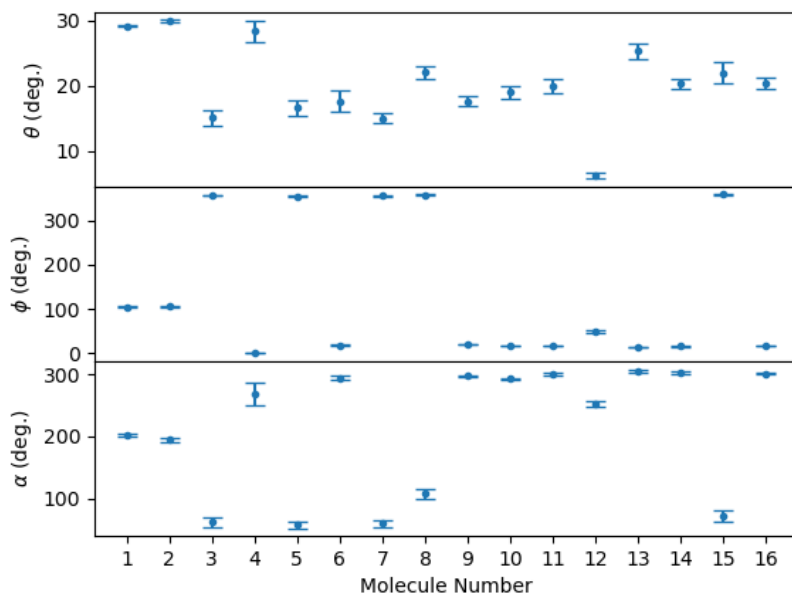

Figure S11: Molecules angles obtained from the global fit procedure. See the article for angles definitions.

We present in Figure S12 the comparison of the results obtained from the global fit procedure to results obtain from detection polarization measurements analyzed with two models : Fourkas[13] and Lethiec et al.[14] The first one considers a dipole emitting in a homogeneous

isotropic medium. The second one considers a dipole emitting in a homogeneous isotropic medium (taken as glass) close to an interface (air).
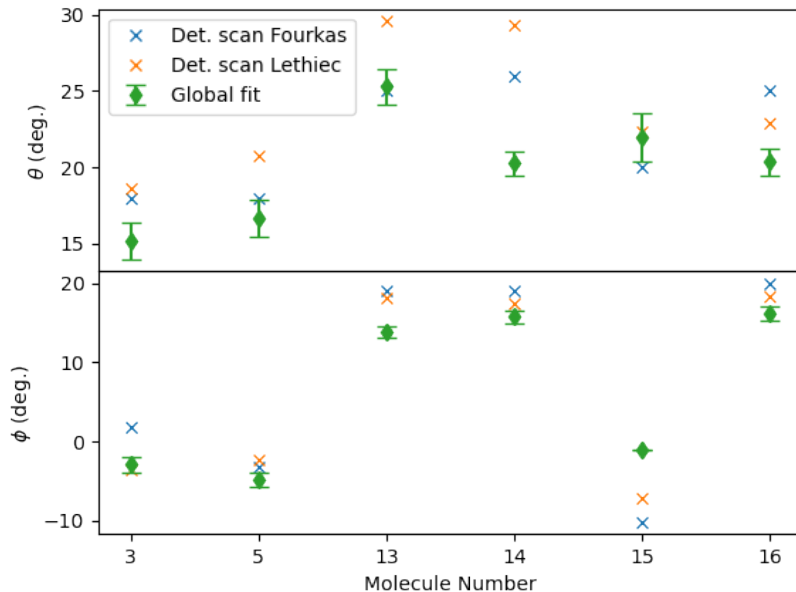

Figure S12: Comparison of angle results obtained from the global fit procedure and polarization detection scan treated with two different methods.

The excitation intensity inside the pT film as well as the angles deduced from the global fit function and analytical models do not take into account the optical index anisotropy of the pT thin film. For our excitation field calculations, we used a refractive index of n=1.8, which is an average between the different directions. As mentioned in Ref,[15] the anisotropy of the matrix also has an effect on the dipole emission pattern. However in our simple configuration (no antenna), the observation of back-focal plane images of single Tr molecule in thin pT film gives results that are very close to isotropic theoretical calculation,[16,17] so we expect the matrix anisotropy to have an negligible effect on our results.

7. Discussion on the pysical origin of molecule populations

As discussed in the main article, what we probe via the σ_{32a} and σ_{32o} deshelving rate is a product of the T_1-T_n absorption cross-section with the triplet to singlet reverse-intersystem crossing rate. The crystal is monoclinic and we expect only one insertion environement of Terrylene in the matrix (a para-terphenyl substitution). The strong difference in the magnitude of σ_{32o} between the ip and oop molecules is thus surprising. We think that another insertion scheme can be possible, and that we end up with one insertion site having an unconstrained Terrylene, and another one having a more strained Terrylene, inducing changes either in the T_1-T_n absorption, or in the r-ISC from T_n to the singlet manifold.

We start with the T_1-T_n absorption alone, considering the ideal case of a planar isolated Tr molecule. Theoretical work by the Nakano group[18] predicts $T_1 - T_5$ and $T_1 - T_6$ transitions with oscillator strength of 0.08 and 0.95 and energies of 2.34 eV and 2.40 eV respectively. This is consistent with the order of magnitude difference observed for the ip molecules, and points to a $T_1 - T_6$ transition dipole moment aligned with the molecule long axis and a $T_1 - T_5$ transition dipole moment aligned with the molecule short axis. In that case, the ip molecules would be the closest to an ideal planar Tr molecule. This deduction suffers however from different biases, as we do not know the broadening of the $T_1 - T_n$ absorption, and their relative contributions at our excitation energy (2.33 eV).

Experimental work by the Müllen group[19] observed two T_1-T_n transitions in a transient absorption experiment in solution, and obtained energies of 2.25 eV and 2.42 eV in benzene, and 2.29 eV and 2.48 eV in cyclohexane, in good agreement with the theoretical work of the Nakano group. However, the intensity of the bands do not agree with the oscillator strength derived in the theoretical results: the low energy extinction coefficient (corresponding to the theoretical 0.08 oscillator strength) is three times higher than the high energy one (corresponding to the theoretical 0.95 oscillator strength). When fitting the experimental data

from Ref.,[19] Fig. 3b, one can extract the contribution of each triplet T_1-T_n absorption at the excitation energy (2.33 eV) and we find a ratio of 2.27. This value is close to the ratio $\sigma_{32a}/\sigma_{32o}$ for oop molecules, which would imply that oop molecules are actually the most planar ones.

Using the available informations, it is thus difficult to infer which of ip or oop has the most planar geometry (or the least constrained insertion site), but we can get an estimate of the r-ISC probability from the T_n states to the singlet manifold. The transient absorption experiment probes directly the (orientation averaged) T_1-T_n transitions, while our experimental scheme probes the succession of a T_1-T_n absorption followed by r-ISC to the singlet manifold. The transient absorption gives values of 1.5×10^{-16} cm^2 at 532 nm (in benzene), while our results give a spatially averaged value of 3×10^{-20} cm^2 range. This gives an estimated r-ISC probability from the T_n states to the singlet manifold in the order of 5×10^{-3}.

We can't rule out the presence of a ^{13}C carbon in Tr (24% from natural abondance). However our study does not provide sufficient number of molecules to confirm this. Another origin can be extra-molecular through the interaction with the pT matrix vibrationnal levels.

References

1. Loudon, R. *The quantum theory of light*; OUP Oxford, 2000.

2. Kulzer, F.; Koberling, F.; Christ, T.; Mews, A.; Basché, T. Terrylene in p-terphenyl: Single-molecule experiments at room temperature. *Chemical Physics* **1999**, *247*, 23–34.

3. Pfab, R. J.; Zimmermann, J.; Hettich, C.; Gerhardt, I.; Renn, A.; Sandoghdar, V. Aligned terrylene molecules in a spin-coated ultrathin crystalline film of p-terphenyl. *Chemical Physics Letters* **2004**, *387*, 490–495.

4. Avlasevich, Y.; Kohl, C.; Müllen, K. Facile synthesis of terrylene and its isomer benzoindenoperylene. *J. Mater. Chem.* **2006**, *16*, 1053–1057.

5. Fleury, L.; Segura, J.-M.; Zumofen, G.; Hecht, B.; Wild, U. Photon statistics in single-molecule fluorescence at room temperature. *Journal of Luminescence* **2001**, *94-95*, 805–809, International Conference on Dynamical Processes in Excited States of Solids.

6. Reynaud, S. La fluorescence de résonance : Etude par la méthode de l'atome habillé. *Annales de Physique* **1983**, *8*, 315–370.

7. Müller, P. Python multiple-tau algorithm (Version 2021.11.12.post15). 2012; `https://pypi.python.org/pypi/multipletau/`.

8. AXELROD, D. Fluorescence excitation and imaging of single molecules near dielectric-coated and bare surfaces: a theoretical study. *Journal of Microscopy* **2012**, *247*, 147–160.

9. Novotny, L.; Hecht, B. *Principles of nano-optics*; Cambridge university press, 2012.

10. Born, M.; Wolf, E. *Principles of optics: electromagnetic theory of propagation, interference and diffraction of light*; Elsevier, 2013.

11. Waxenegger, J.; Trügler, A.; Hohenester, U. Plasmonics simulations with the MNPBEM toolbox: Consideration of substrates and layer structures. *Computer Physics Communications* **2015**, *193*, 138–150.

12. Beveratos, A.; Brouri, R.; Gacoin, T.; Poizat, J.-P.; Grangier, P. Nonclassical radiation from diamond nanocrystals. *Physical Review A* **2001**, *64*, 061802.

13. Fourkas, J. T. Rapid determination of the three-dimensional orientation of single molecules. *Opt. Lett.* **2001**, *26*, 211–213.

14. Lethiec, C.; Laverdant, J.; Vallon, H.; Javaux, C.; Dubertret, B.; Frigerio, J.-M.; Schwob, C.; Coolen, L.; Maître, A. Measurement of Three-Dimensional Dipole Orienta-

tion of a Single Fluorescent Nanoemitter by Emission Polarization Analysis. *Phys. Rev. X* **2014**, *4*, 021037.

15. Zhang, P.; Ren, P.-L.; Chen, X.-W. On the emission pattern of nanoscopic emitters in planar anisotropic matrix and nanoantenna structures. *Nanoscale* **2019**, *11*, 11195–11201.

16. Buchler, B. C.; Kalkbrenner, T.; Hettich, C.; Sandoghdar, V. Measuring the Quantum Efficiency of the Optical Emission of Single Radiating Dipoles Using a Scanning Mirror. *Phys. Rev. Lett.* **2005**, *95*, 063003.

17. Lieb, M. A.; Zavislan, J. M.; Novotny, L. Single-molecule orientations determined by direct emission pattern imaging. *J. Opt. Soc. Am. B* **2004**, *21*, 1210–1215.

18. Minami, T.; Ito, S.; Nakano, M. Theoretical Study of Singlet Fission in Oligorylenes. *The Journal of Physical Chemistry Letters* **2012**, *3*, 2719–2723, PMID: 26295897.

19. Meyer, Y.; Plaza, P.; Müllen, K. Ultrafast spectroscopy of soluble terrylene and quaterrylene. *Chemical Physics Letters* **1997**, *264*, 643–648.